nature physics

SUPPLEMENTARY INFORMATION

DOI: 10.1038/NPHYS2049

Dirac cones reshaped by interaction effects in suspended graphene

D. C. Elias *et al*

#1. Experimental devices

Graphene monolayers were obtained by micromechanical cleavage of graphite on top of an oxidized Si wafer [S1]. In this work, we specially selected long and narrow crystals (typically, 2 to 4 μm wide) which allowed us to avoid dry etching of graphene mesas. Two-terminal devices such as shown in Fig. 2 of the main text were then designed and fabricated by using standard lithography and deposition techniques. The 300 nm SiO_2 layer was partially etched in a buffered HF solution to leave graphene hanging above the substrate. The metal leads (5 nm Cr followed by 100 nm of Au) remained not fully etched underneath and served as a mechanical support. These fabrication procedures are similar to those described in refs. [S2-S5].

The current annealing was performed in situ, in a liquid-helium bath by applying voltage between adjacent contacts. Current densities of ~1 mA/μm were necessary to heat suspended graphene locally to T >600°C [S5]. Our devices either fail or anneal after a minor (<1%) increase in applied voltage, which we believe is an indication that the real T of annealing could be even higher than suggested in ref. [S5].

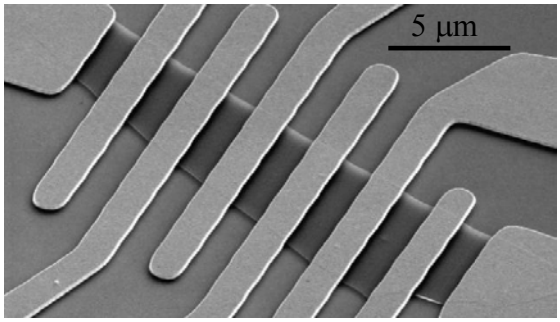

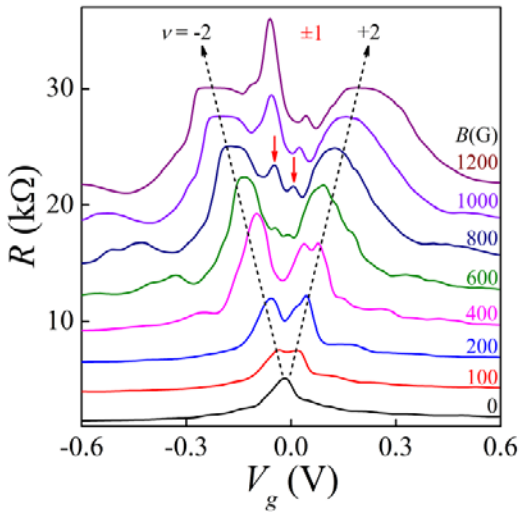

Figure S1. Our graphene devices. Left – Scanning electron micrograph of another suspended device, different from the one shown in Fig. 2a. Right – Typical behaviour of $R(V_g)$ measured at 2K. The curves are shifted for clarity. The QHE in the two probe geometry is known to lead to plateaux in R at $h/\nu e^2$. Such QHE plateaux are clearly seen in our devices below 0.1T. The dominant QHE plateau (filling factor $\nu = \pm 2$) at $R \approx 12.8 k\Omega$ is first formed at negative gate voltages where μ is somewhat higher. Additional peaks at lower $|V_g|$ correspond to $\nu = \pm 1$ and indicate either spin or valley splitting.

DOI: 10.1038/NPHYS2049

Figure S1 shows two-terminal resistance R as a function of gate voltage V_g in different magnetic fields B. We refer to our measurements as two-terminal because the supporting metal contacts overlap with the current path (Fig. S1), that is, they are invasive [S6,S7]. In this measurement geometry, we found little difference whether we used two- or four-probe measurement geometry because of the relatively small resistance of the metal leads.

As one can see in Figure S1, the Landau level splitting occurs at B ~100 G (red and blue curves). The observation of SdHO requires $\mu B \approx 1$, which allows us to estimate quantum mobility μ as ~10^6 cm^2/Vs [S3,S4,S8]. This value is in good agreement with the field-effect μ found from changes in conductivity σ as a function of n in zero B [S4] (also, see Fig. S2). As a further indication of the graphene quality, one can see that the first quantum Hall effect (QHE) plateau develops at 600 G for holes (green curve; negative V_g) and becomes fully formed for both electrons and holes at 1000 G (violet). Also, the 4-fold degeneracy of the lowest LL becomes lifted already at ~600 G (green).

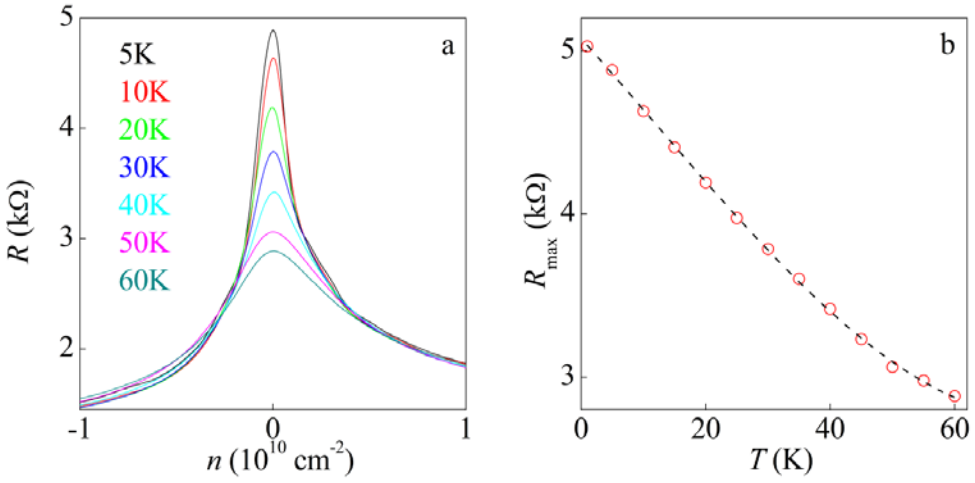

Figure S2. No discernable gap in neutral graphene. (**a**) – R as a function of concentration n in a suspended device at various T in zero B. The peak at the Dirac point continues to sharpen with decreasing T but R remains finite, with no sign of a gap: that is, $R(T)$ does not diverge at $T \to 0$. (**b**) – The device's maximum resistance as function of T. The points are the experimental data and the dashed curve is a guide to the eye. The practically linear dependence $R(T)$ is puzzling and may be related to the transition from the dependence $R \propto 1/T^2$ found at high T (due to thermally generated carriers at the NP) to the pseudo-diffusive regime with a finite conductivity in the limit of low T.

Charge inhomogeneity δn is usually estimated from smearing of the resistance peak near the NP. However, in our devices, the peak continues sharpening down to 2 K (Fig. S2), the lowest T in the current experiments. This shows that the thermal generation of electrons and holes at the NP

dominates any remnant charge inhomogeneity, which yields δn less than ~10^8 cm^{-2}, that is of about one electron per square μm. In order to extract cyclotron mass m_c it was necessary to measure SdHO at many different T. This effectively led to δn being determined by T rather than real inhomogeneity and limited our m_c measurements to $n \geq 10^9$ cm^{-2}. Furthermore, the smooth monotonic behaviour of R as a function of both n and T (see Fig. S2) implies that, except for the discussed logarithmic corrections, no dramatic reconstruction of the Dirac spectrum occurs at E down to 1 meV ($n \approx 10^8$ cm^{-2}). Otherwise, one would expect to observe some anomalies in $R(n,T)$ whereas the presence of an energy gap larger than ~0.1 meV would be seen as diverging $R(T \to 0)$.

#2. Analysis of Shubnikov–de Haas oscillations

We have measured the cyclotron mass m_c in graphene by analysing T dependence of SdHO. This well-established approach has widely been used in literature [S9-S10]. In the case of graphene, the approach provided accurate measurements of m_c which retrospectively were found in good agreement with the results obtained by other techniques (e.g., magneto-optics and tunnelling microscopy). In brief, our procedures involved measurements of suspended graphene's conductance $G = 1/R$ as a function of n at a given B. Then, we changed T and repeated the measurements. T and B were always chosen to keep far away from the QHE regime so that changes in conductance $\Delta G << G$.

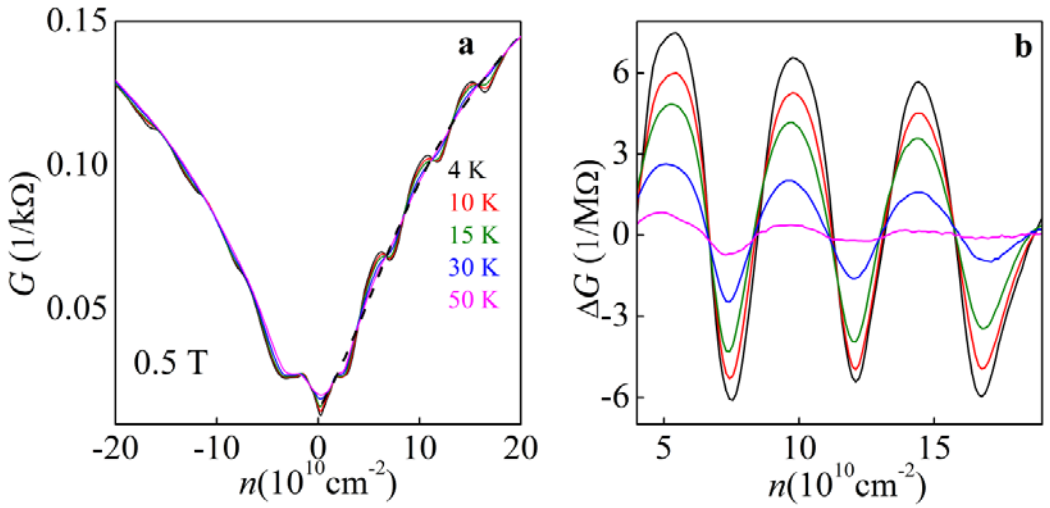

Figure S3. (a) – $G(n)$ for a suspended graphene device in B =0.5 T at several T. The dashed curve indicates the smooth polynomial background. (b) – Curves from (a) after the subtracting the background.

Examples of our raw data are shown Figure S3a. SdHO are clearly seen on top of the standard V-shaped background. This background is smooth and, for easier analysis, can be subtracted. We have done this separately for electrons and holes. To standardise the procedures, we normally defined the

DOI: 10.1038/NPHYS2049

background by fitting a 4th-order polynomial to one of high-T curves $G(n)$ with no discernable oscillations, as illustrated in Fig. S3a. The subtraction resulted in curves such as shown in Fig. S3b. The SdHO amplitude was then calculated as the difference between ΔG in maxima and minima. This yielded the data such as shown in Fig. 2a of the main text. Typically, we used 10 different T to obtain each value of m_c. The results were practically independent of the choice of subtracted background and other procedural details, essentially due to the fact that we analyzed the difference between minima and maxima.

#3. Influence of a dielectric substrate

As found in many experiments, graphene on SiO_2 exhibits the Fermi velocity $v^*_F \approx 1.05 \pm 0.1 \times 10^6$ m/s for the typically accessible range of $n \sim 10^{12}$ cm^{-2}. The measurements for suspended graphene reported in the main text show a slightly higher v_F (15 to 25%) for the same range of n. This disagreement can be attributed to the absence of dielectric screening in the suspended devices. To prove this and exclude any systematic error arising due to the use of devices with drastically different mobilities (μ differ by a factor of 100 for suspended graphene and graphene on SiO_2), we performed measurements of $m_c(n)$ for graphene on boron nitride (GBN). The latter devices allow $\mu > 100{,}000$ cm^2/V and, at the same time, e-e interactions are screened in a manner similar to the case of graphene on SiO_2 (boron nitrite exhibits $\varepsilon_s \approx 5$ [S11]).

Our GBN devices were fabricated as described in refs. [S12,S13] and one of the studied devices is shown in Fig. S4. To find m_c, we performed the same measurements and analysis as described in the previous chapter. The resulting dependence $m_c(n)$ is shown in Fig. S4. The accessible range of n was limited to $\geq 10^{11}$cm^{-2} due to charge inhomogeneity that was smaller than in graphene on SiO_2 but still significant, in agreement with refs. [S13,S14]. The dashed curve corresponds to a constant $v_F = v^*_F$ and provides an excellent description of our data within this limited range of n, similar to the case of graphene on SiO_2. This strongly supports the argument that v_F in graphene on a substrate is lower than in suspended graphene due to dielectric screening in the former case.

To check our analysis of the renormalized spectrum for consistency, the solid and dotted curves in Figure S4 show $m_c(n)$ calculated by using to equation (2). The dotted line is the same theory curve shown in Figs. 2c and 3 of the main text for suspended graphene, which corresponds to the case of $\varepsilon = 1$ and $\Lambda \approx 3$eV. On the other hand, the solid line was calculated by using the same equation and only adding the dielectric screening due to boron nitride with no change in other parameters. The agreement between the experiment and theory is impressive and shows that our theoretical

description is able to explain not only the n dependence of the Fermi velocity but, also, its dependence on dielectric screening.

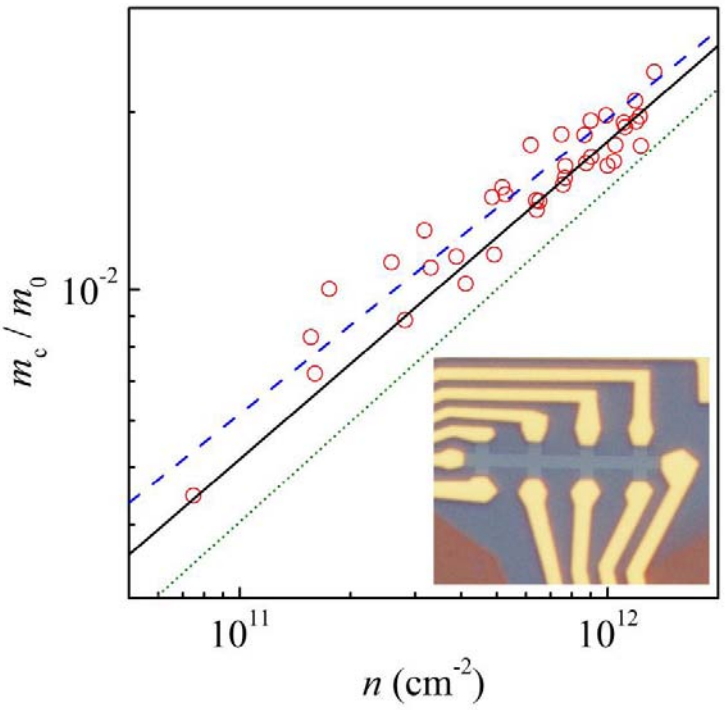

Figure S4. Cyclotron mass as function of n for graphene on boron nitride. The symbols are experimental data; the dashed line is the non-interacting behaviour with constant $v_F = v^*_F$. The RGT approach, which is used in the main text to describe $m_c(n)$ in suspended graphene over a wide range of n, is also consistent with the limited-range data for GBN devices. The dotted curve is given by equation (2) of the main text (ε=1; Λ =3eV) whereas the solid one is for ε_s=5; Λ =3eV (no fitting parameters). The inset shows an optical micrograph of a Hall bar device made from graphene deposited on BN (no encapsulating top layer [S13]). For clarity, the contrast of the 1μm wide graphene mesa was digitally enhanced.

#4. Interaction renormalization of the Dirac spectrum in various approximations

Near the NP, screening is weak due to the low density of states and completely suppressed in neutral graphene because the density of states goes to zero. As a result, electronic levels become increasing affected by e-e interactions as their energy approaches the Dirac point. The Hartree-Fock correction to the quasiparticle energy is given by

$$\delta E \approx \pm \int d^2\vec{k}' \frac{2\pi e^2}{\varepsilon|\vec{k}-\vec{k}'|}\left(\frac{1}{2} \pm \frac{\vec{k}\cdot\vec{k}'}{|\vec{k}||\vec{k}'|}\right) \approx \pm \frac{e^2}{4\varepsilon}\ln\left(\frac{k_\Lambda}{|\vec{k}|}\right) \qquad \text{(S1)}$$

where k_Λ is the upper limit in the momentum integral, and the signs ± correspond to electrons and holes, respectively. This equation yields a change in the Fermi velocity δv_F which becomes a function of momentum $\vec{k}$

$$\delta v_F \approx \frac{e^2}{4\varepsilon}\ln\left(\frac{k_\Lambda}{|\vec{k}|}\right) \qquad \text{(S2).}$$

DOI: 10.1038/NPHYS2049

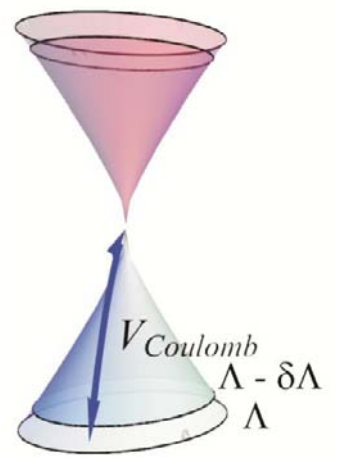

Figure S5. Sketch for the Renormalization Group procedure used to explain the experimental observations. Coulomb interactions between low- and high- E states deplete the electronic spectrum near the Dirac point.

An improvement over the Hartree-Fock approximation can be achieved by calculating changes in v_F for low-E quasiparticles, which are induced by their interaction with high-E excitations in the interval of energies $\Lambda-\delta\Lambda \le E \le \Lambda$ and defining a new model for the electronic spectrum in which these excitations are removed, as schematically shown in Fig. S5. Within this model, v_F is described by

$$\hbar v_F(\Lambda-\delta\Lambda) \approx \hbar v_F(\Lambda) + \frac{e^2}{4\varepsilon}\frac{\delta\Lambda}{\Lambda} \tag{S3}$$

Or, alternatively

$$\hbar k \frac{\partial v_F}{\partial k} = -\frac{e^2}{4\varepsilon} \tag{S4}.$$

This result reproduces equation (1) in the main text. Using the same analysis, it can be shown that there is no need to modify other parameters in the Hamiltonian. This scheme defines the RGT transformation that is exact in the limit $\alpha = e^2/\hbar v_F << 1$. The self energy diagram that gives rise to eq. (1) is shown in Fig. S6a. However, the above limit is not valid for graphene where the effective fine structure constant $\alpha \approx 2$. The fact that α is of order unity makes it problematic to use the standard expansion methods. This problem can be overcome by using the expansion in powers of $1/N_f$ as described below.

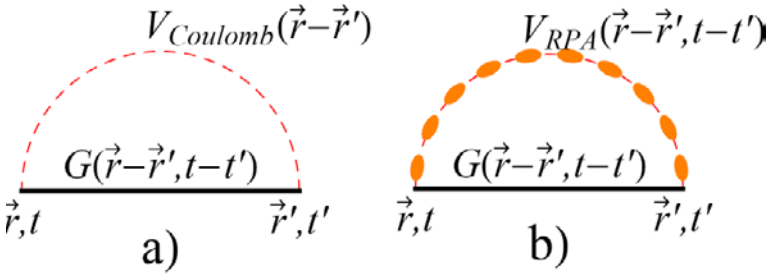

Figure S6. (a) – Diagram that leads to eq. (1) of the main text. (b) – The diagram takes into account self-screening.

Equations (1) and (S1-S4) include only screening effects due to environment of the graphene sheet, which is described by the dielectric constant ε. The intrinsic screening by charge carriers can also be added in a phenomenological way by redefining ε and introducing ε_G as discussed in the main text. Alternatively, a better description can be achieved by self-consistently including the screening

processes into the interaction line in Fig. S6a. The resulting diagram is shown in Fig. S6b, and this leads to equation (2) of the main text. Furthermore, it can be shown that the infinite summation of polarization bubbles in the second diagram results in the approximation that becomes exact if $N_f >> 1$. In graphene, $N_f = 4$ so that the approximation's accuracy is comparable to similar calculations used in quantum chromodynamics [S15].

The analysis of experimental results in the main text is mainly based on the above eq. (2) because this approach does not require any prior knowledge of the electronic polarizability, α or ε_G. Furthermore, eq. (2) allows us to determine the value of ε_G for different n, which has become a subject of debate after anomalously large $\varepsilon_G \approx 15$ were reported [S16]. We have found significantly smaller ε_G (see the main text). This is in agreement with the RGT expectations and, also, the measurements of electron-plasmon satellites ("plasmarons"), which were reported in ref. [S17] and yielded the bare fine structure constant $\alpha \approx 2.2$ (cf. the best fits to our data gives $\alpha \approx 2.4$).

Finally, it is instructive to compare the renormalized Dirac spectrum inferred from our measurements and shown in Fig. 1 with the excitation spectra modified by interactions and schematically shown in Fig. 1H of ref. [S17]. In our case, we probe v_F as function of n (or the Fermi energy E_F) and its value changes each time we change the low energy cut-off, that is, E_F. The spectrum under the Fermi surface is expected to be linear but its slope (that is, v_F) changes from measurement to measurement. In ref. [S17], the excitation spectra for Dirac fermions are probed underneath the Fermi surface and the cut-off is fixed for all E by either a given n or excitations' energy, whichever value is larger. There is no disagreement between the two figures: these are just the spectra referring to different many-body phenomena.

#5. Influence of disorder

The RGT flow that describes the dependence of v_F on energy leads to changes in this parameter, which can be comparable to v^0_F, the initial values of the parameter itself. On the other hand, other couplings such as electron-phonon [S18] and electron-plasmon interactions [S17] can be treated within a perturbation theory because they do not lead to logarithmic divergences. Therefore, it can be expected that their effect on the Fermi velocity does not exceed a fraction of its value and, accordingly, they cannot explain the large enhancement observed in the experiment. The only other interaction that can lead to logarithmic renormalization is the coupling to some types of scalar and gauge random disorder [S19-S21]. However, the arising corrections have the opposite sign with

DOI: 10.1038/NPHYS2049

respect to that due to electron-electron interactions. Furthermore, the disorder can be described by the dimensionless parameter

$$\Delta \sim \langle V^2 \rangle (l/v_F)^2 \quad \text{(S5)}$$

where $\langle V^2 \rangle$ gives the average value of the disorder, and l is the range over which it is correlated. This gives rise to a scattering time τ

$$h/\tau \sim \Delta \times E_F \quad \text{(S6)}$$

where E_F is the Fermi energy. In order to significantly change the effect of electron-electron interaction, the value of Δ should be comparable to $e^2/\hbar v_F$. The long mean free path, characteristic of the suspended graphene studied in this work, rule out the existence of such strong disorder.

Supplementary References

[S1] K. S. Novoselov *et al*. *PNAS* **102**, 10451 (2005).

[S2] X. Du *et al*. *Nature Nanotech.* **3** 491 (2008).

[S3] K. I. Bolotin *et al. Solid State Commun.* **146** 351 (2008).

[S4] E. V. Castro et al. *Phys. Rev. Lett.* **105**, 266601 (2010).

[S5] K. I. Bolotin et al. *Nature* **462** 351 (2008).

[S6] P. Blake *et al*. *Solid State Commun* **149**, 1068 (2009)

[S7] J. R. Williams *et al*. *Phys. Rev. B.* **80**, 045408 (2009)

[S8] M. Monteverde *et al*. *Phys. Rev. Lett.* **104**, 126801 (2010).

[S9] J. L. Smith and P. J. Stiles, Phys. Rev. Lett. 29, 102–104 (1972)

[S10] W. Pan and D. C. Tsui, Phys. Rev. B 59, 10208–10211 (1999)

[S11] R. V. Gorbachev *et al*. *Small* **7**, 465 (2011).

[S12] C. R. Dean *et al*. *Nature Nanotech.* **5**, 722 (2010).

[S13] A. S. Mayorov *et al*. *Nano Lett.* to appear (2011) (see arXiv:1103.4510).

[S14] J. Xue *et al*. *Nature Mater.* **10**, 282 (2011)

[S15] S. Coleman, *Aspects of Symmetry*, Cambridge University Press (1985).

[S16] J. P. Reed et al. *Science* **330**, 805 (2010).

[S17] A. Bostwick et al. *Science* **328**, 999 (2010).

[S18] C.-H. Park et al. *Phys. Rev. Lett.* **99**, 086804 (2007).

[S19] T. Stauber et al. *Phys. Rev. B* 71, 041406, (2005).

[S20] M. S. Foster and I. L. Aleiner, *Phys. Rev. B*, **77**, 195413 (2008).

[S21] I. F. Herbut et al. *Phys. Rev. Lett.* **100**, 046403 (2008).